

WARM ABSORBERS IN AGN: A MULTI-TEMPERATURE WIND

JULIAN H. KROLIK

Department of Physics and Astronomy, Johns Hopkins University, Baltimore, MD 21218
jhk@pha.jhu.eduGERARD A. KRISS¹Space Telescope Science Institute, 3700 San Martin Drive, Baltimore, MD 21218
gak@stsci.edu*Accepted for publication in ApJ, 18 July 2001*

ABSTRACT

Although soft X-ray absorption features in AGN were discovered almost ten years ago, the nature and location of the gas creating them has remained controversial. Guided by the results of recent high-resolution X-ray spectroscopy, we argue that these features are created in a multi-temperature wind whose source of matter is photoionized evaporation from the inner edge of the obscuring torus often found surrounding AGN. Photoionized evaporation in the presence of a copious mass source locks the ratio of ionizing intensity to pressure to a critical value. However, a broad range of temperatures can all coexist in equilibrium for this value of the ratio of ionizing intensity to pressure. Consequently, the flow is expected to be strongly inhomogeneous in temperature. The inferred distance of this material from the source of ionizing radiation depends on how much matter exists at the highest-obtainable temperature. This distance can be measured by monitoring how ionic column densities respond to changes in the ionizing continuum on timescales of days to years.

Subject headings: Galaxies: Active — Galaxies: Nuclei — Galaxies:Seyfert — Galaxies: Quasars: Absorption Lines — X-rays: Galaxies — Ultraviolet: Galaxies

1. INTRODUCTION

X-ray spectra of active galactic nuclei (AGN) commonly reveal intrinsic absorption by highly ionized or “warm” gas. First seen in ROSAT and ASCA spectra (Turner et al. 1993; Reynolds et al. 1995; Reynolds 1997; George et al. 1998b), absorption edges of O VII and O VIII can be found in half or more of all type 1 Seyfert galaxies, and in a few quasars (Mathur et al. 1994).

The location of this gas is still unknown. Suggestions range all the way from the broad-line region (BLR), possibly as close as ~ 0.01 pc from the nucleus, to distances of 10 pc or more. Rapid apparent column density variations have been interpreted as suggesting locations in the BLR (Reynolds et al. 1995; George et al. 1998b). On the other hand, the same data also indicate that at least some of the gas may be much farther away (Otani et al. 1996). Others have placed the gas at ~ 1 pc in the scattering region posited by Seyfert galaxy unification schemes (Krolik & Kriss 1995), or a factor of 10 farther away (Bottorff et al. 2000). Morales et al. (2000) suggested that the absorber is spread all the way from < 0.05 pc to > 1 pc. Still less is known about the origin, dynamics, or destiny of the gas producing warm absorber features. Some of the diverse suggestions include: evaporation off “bloated stars” in the BLR (Netzer 1996); gas, evaporated off the torus obscuring the nucleus, that becomes the scattering gas seen in type 2 Seyfert galaxies (Krolik & Kriss 1995); and a wind driven off the accretion disk (Elvis 2000; Bottorff et al. 2000).

With the launch of *Chandra* and *XMM-Newton*, we now have access to data of far better quality, and may reasonably hope to settle some of these outstanding questions. Most notably, the high resolution available with the grating spectrographs on these spacecraft has permitted detection of resonance line features (Kaastra et al. 2000; Kaspi et al. 2000; Kaspi et al. 2001; Lee et al. 2001; Collinge et al. 2001). As we will show later, measurement (or even bounds) on line widths and shifts (i.e., relative to the host galaxy rest-frame) can provide powerful hints toward answering many of the questions just posed. It is our object here to show how this new data points us toward a revision of the “scattering wind” model. Because this model makes specific predictions about the character of variability on measurable timescales, it should be easily testable in the near future.

2. THE MODEL: A CRITICAL-PRESSURE WIND

2.1. Phenomenological guidance

Measured column densities of different ionization stages seen in absorption can be used to constrain photoionization properties of the absorbing gas under the assumption that the species involved are in ionization (and optionally also thermal) balance. The relative abundances of different species fix the ionization parameter $\xi \equiv L_{ion}/nr^2$; the strengths of the lines and edges fix the hydrogen column density N . Here the ionizing luminosity L_{ion} is conventionally taken to be the luminosity between 1 and 1000 Ryd, n is the hydrogen volume density, and r is the distance from the nucleus to the photoionized gas. Other, closely-related, versions of the ionization parameter are also used, e.g., $U_{oxygen} \equiv \int_{0.538}^{10} d\epsilon(L_{\epsilon}/4\pi r^2 enc)$

¹ also, Department of Physics and Astronomy, Johns Hopkins University, Baltimore, MD 21218

(George et al. 2000), where photon energy ϵ is measured in keV and L_ϵ is the luminosity per unit energy. Its precise relation to ξ depends on the shape of the continuum spectrum.

These quantities can then be used (Turner et al. 1993) to estimate the fractional radial thickness occupied by absorbing gas

$$\Delta r/r = \xi N r / L_{ion}. \quad (1)$$

Placing the gas close to the nucleus implies a highly “clumped” structure, whereas larger distances imply a more volume-filling configuration. The gas cannot, in any case, be farther than $r_{max} = L_{ion}/(N\xi)$ because $\Delta r/r \leq 1$. Simple photoionization-fitting cannot distinguish between a clumpy and a smooth configuration; it can only define the link between the degree of clumpiness (or smoothness) and the distance from the nucleus to the absorbing gas.

The most commonly observed features (especially in ASCA data) are those associated with O VII and O VIII (Reynolds 1997; George et al. 1998b). In order to make them reasonably abundant, $\xi \sim 10 - 100$. For this reason, many photoionization models of warm absorbers have suggested values of ξ in this range, e.g., (Brandt et al. 1997; Reynolds 1997; George et al. 1998b; Mathur et al. 1997). On the other hand, more recent work has detected many other species of higher ionization level (Collinge et al. 2001), suggesting that there may be substantial amounts of gas with $\xi \sim 100 - 1000$ (Kaastra et al. 2000; Kaspi et al. 2001). The maximum distance of the absorbing region in a Seyfert galaxy is then $r_{max} \sim 30 L_{ion,44} N_{22}^{-1} \xi_{100}^{-1}$ pc, where the fiducial quantities (10^{44} erg s $^{-1}$ for L_{ion} , 10^{22} cm $^{-2}$ for N , and 100 for ξ) have been chosen to be representative of those commonly inferred.

Line profiles convey additional information. For example, Kaspi et al. (2001) find that the absorption lines they detect have a mean blueshift relative to the galaxy’s systemic velocity of 610 km s $^{-1}$. The gas must, therefore, possess a net flow toward us. The associated mass outflow rate is

$$\dot{M}_{out} = 4\pi C \mu_H N r v = 0.72 C N_{22} r_{pc} (v/500 \text{ km s}^{-1}) M_\odot \text{ yr}^{-1}, \quad (2)$$

where its covering fraction around the nucleus is C , μ_H is the mean mass per H atom, r_{pc} is the radius normalized to 1 pc, and v is the mean outflow speed. Interestingly, the ratio of the outflow rate to the accretion rate required to power the nuclear luminosity can be ~ 100 :

$$\frac{\dot{M}_{out}}{\dot{M}_{acc}} = 600 C v_{500} \left(\frac{\eta_{acc}}{0.1} \right) \left(\frac{r}{r_{max}} \right) \left(\frac{L_{ion}/L_{bol}}{0.5} \right) \left(\frac{\xi}{100} \right)^{-1}, \quad (3)$$

where L_{bol} is the bolometric luminosity and η_{acc} is the accretion efficiency (cf. Krolik & Begelman 1986, Reynolds 1997).

The widths of the absorption lines appear to be similar to their blueshifts; many absorption lines also have emission components to the red (i.e., “P Cygni”-type profiles) (Kaspi et al. 2001). The fact that the emission components are centered at the systemic velocity and have widths comparable to the blueshifts is most simply understood as indicating that emission and absorption are made by gas with similar properties, but that the line emission sources are located to the side of and behind the continuum source.

All measures of gas velocity are roughly an order of magnitude smaller than the typical speeds of gas in the BLR. Following the common rule-of-thumb that speeds diminish at increasing distance from the central black hole, this contrast would suggest that the absorbing gas is rather more distant than the BLR (Kaspi et al. 2000). Still more speculatively, if velocities scale $\propto r^{-1/2}$, the warm absorber material must be ~ 100 times farther from the nucleus than the BLR, i.e., in NGC 3783 it must be parsecs from the nucleus if we adopt the reverberation-mapping estimate of its BLR scale (Reichert et al. 1994).

On the basis of this evidence (modest velocity outflow, maximum distance $\sim 30 L_{ion,44}$ pc, moderately high ionization) and the comparisons to observations presented in §3, we find the most natural model to be a close relation to the one proposed by Krolik & Kriss (1995). Again, we identify the warm absorber with the hot scattering gas of Seyfert galaxy unification models. However, as discussed in the next subsection, our view of its thermodynamic state is somewhat different from the one expressed six years ago.

2.2. Thermodynamics of the warm absorber

In this model, the origin of the warm absorber gas is material evaporated off the inner edge of the toroidal obscuration. The position of this inner edge is determined by a combination of dust sublimation and photoionization (Pier & Voit 1995), but is expected to be $\sim 1 L_{ion,44}^{1/2}$ pc. The existence of rings of H $_2$ O masers at approximately this distance (Greenhill et al. 1996) is in keeping with this expectation. Thus, the source for the warm absorbing gas would be roughly this far from the nucleus.

The thermodynamics of this evaporating gas are best described by an ionization parameter framed in terms of the gas pressure, such as $\Xi \equiv L_{ion}/(4\pi r^2 c n k T)$ (Krolik, McKee & Tarter 1981). When Ξ exceeds a critical value ($\Xi_c \sim 10 - 30$ for typical AGN spectra), the gas is no longer capable of maintaining a cool ($\sim 10^4$ K) equilibrium temperature; instead its equilibrium temperature rises very rapidly with increasing Ξ until it approaches the Compton temperature, which in AGN is generally several orders of magnitude greater.

The detailed character of this rise depends on the specific shape of the continuum (and also on details of atomic physics that are imperfectly known), but its qualitative behavior—a nearly vertical rise from temperatures $\sim 3 \times 10^4$ K to $\sim 10^6$ K at $\Xi \simeq \Xi_c$ —is the same for almost any AGN-like spectrum. In Figure 1 we show $T(\Xi)$ (as computed using Version 2.1 of XSTAR, Kallman 2000) for two continuum shapes based on data from the type 1 Seyfert galaxy NGC 3783, one suggested

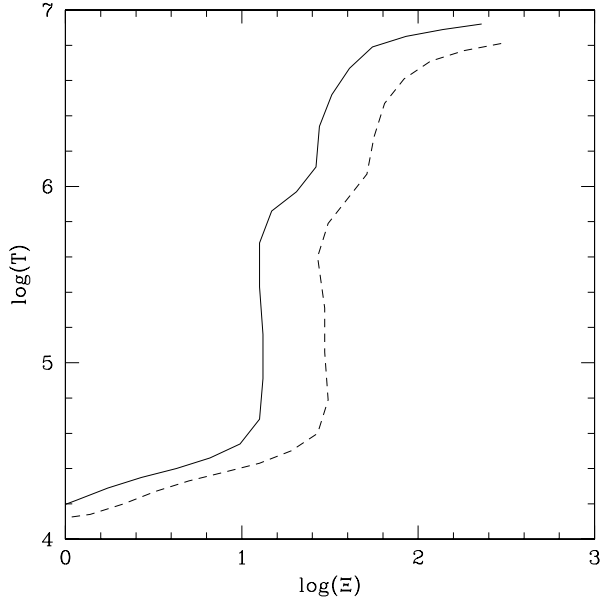


Fig. 1.—The equilibrium temperature as a function of Ξ for the Kaiser et al. (2001) spectrum of NGC 3783 (solid curve) and the Kaspi et al. (2001) spectrum (dashed curve).

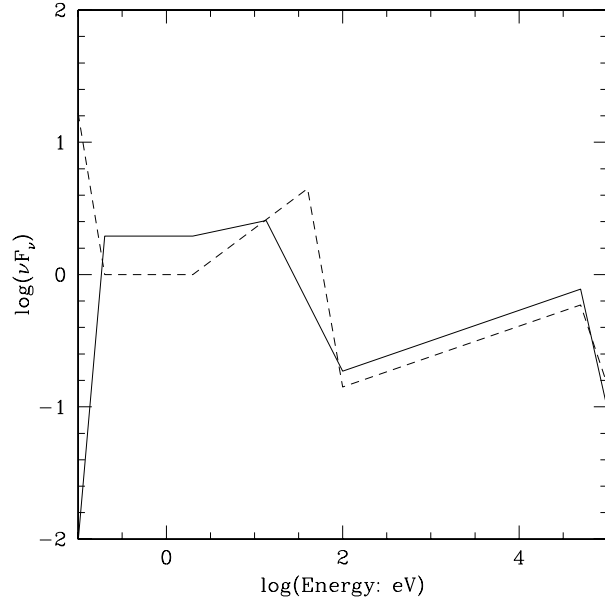


Fig. 2—Proposed continuum shapes for NGC 3783: solid curve by Kaiser et al. (2001), dashed curve by Kaspi et al. (2001). Both are plotted in terms of flux per logarithmic frequency interval, νF_ν ; the vertical scale is arbitrary.

by Kaiser et al. (2001), the other by Kaspi et al. (2001). The rise is very similar for both spectra; almost the only difference is the offset in Ξ_c . The fiducial $\xi = 100$ corresponds to a temperature part way up this rise, 1.5×10^5 K for the Kaiser et al. spectrum, 5.5×10^4 K for the Kaspi et al. spectrum. In terms of ξ , the vertical portion of the equilibrium curve runs from $\xi \simeq 10$ to $\xi \simeq 1000$ in the case of the Kaiser et al. spectrum, but from $\xi \simeq 40$ to $\xi \simeq 1500$ for the Kaspi et al. spectrum.

In this paper we are primarily interested in material near and outside the obscuring torus. In keeping with theoretical expectations that the torus should reradiate a substantial portion of the nuclear luminosity in the infrared, we have required that in each spectrum the luminosity at energies below 2 eV match the ionizing luminosity. No alteration in the Kaiser et al. spectrum was necessary to accomplish this, but to achieve this with the Kaspi et al. spectrum we added a new component at 0.1 eV. Both spectra are shown in Figure 2. The additional infrared intensity makes little difference to the equilibrium curve at temperatures below $\sim 10^6$ K; the primary effect is to reduce the Compton temperature and create the “jog” toward higher Ξ in the range $1 - 3 \times 10^6$ K. Closer to the nucleus, the infrared intensity would be relatively weaker, leading to a higher Compton temperature and a longer section of nearly-vertical temperature rise. Throughout the remainder of this paper, specific numbers derived from photoionization calculations assume the Kaiser et al. spectral shape.

Places where the slope $dT/d\Xi > 0$ are stable against isobaric thermal perturbations, but places where the curve “doubles back” (i.e., where $dT/d\Xi < 0$) are thermally unstable. As shown by the curves of Figure 1, near the obscuring torus there is a significant stretch of the equilibrium curve where the sign of $dT/d\Xi$ is ill-defined because the temperature rises almost exactly vertically: $d\Xi/dT \simeq 0$ for $10^{4.5}$ K $\lesssim T \lesssim 10^{5.9}$ K (and $|d\Xi/dT|$ remains very small up to $T \sim 10^{6.5}$ K). This region is therefore better described as having approximately marginal stability. That is, thermal fluctuations neither grow nor decay exponentially; there is little feedback in either sense. Although the equilibrium curves are never exactly vertical locally, because the overall sense is very nearly vertical, tiny pressure perturbations in regions that are nominally stable can nonetheless lead to large temperature changes. Likewise, temperature perturbations in regions of nominal instability do not lead to arbitrarily large temperature changes—at constant pressure, material rises or falls along a line of constant Ξ , and cannot go far before intersecting the equilibrium curve again, this time on a locally stable segment. It is in this sense that we describe this portion of the equilibrium curve as being “marginally stable”.

The reason to pay such close attention to the character of equilibria with $\Xi \simeq \Xi_c$ is that when there is a copious source of gas available for rapid heating (as the obscuring torus provides in this model), rather than being a special value, Ξ_c is a preferred value of the ionization parameter. Suppose that the pressure in the gas at the illuminated face of the torus were very low, so that $\Xi > \Xi_c$. Then this gas would be subject to strong net heating. As its temperature rises, it expands and its opacity drops sharply. Deep inside the torus, the large continuum optical depth protects the gas and keeps it relatively cool (the most likely temperature is $\lesssim 10^3$ K: Krolik & Lepp 1989, Neufeld et al. 1994), but as the opacity of matter at the illuminated edge is eliminated, new gas is exposed and becomes available for “evaporation”. As more and more gas is removed from the torus and added to the hot phase, the pressure of the hot phase rises because (as we shall

show shortly), its heating time is much shorter than the flow time. Eventually, the pressure rises high enough that Ξ falls to Ξ_c . Conversely, if the ambient pressure were so high that $\Xi < \Xi_c$, gas outside the torus would cool and condense, diminishing the pressure.

Thus, where the gas is injected, the ionization parameter is fixed at Ξ_c . Moreover, with one relatively modest proviso, it remains at that value even as the gas flows away from its injection point. So long as its ionization and thermal equilibration times are short compared to the flow time, the gas must follow the equilibrium curve. Because the equilibrium curve lies along the vertical line $\Xi = \Xi_c$ until the temperature exceeds $\sim 10^6$ K, the gas's ionization parameter remains fixed at that value until the majority of its mass reaches high temperatures.

In fact, both the ionization and thermal balance timescales are indeed considerably shorter than the flow time over a wide range of conditions. The flow timescale $t_{flow} \equiv r/v \sim 6 \times 10^{10} r_{pc} (v/500 \text{ km s}^{-1})^{-1}$ s. On the other hand, the thermal equilibration time $t_{cool} \sim 2 \times 10^7$ s for our fiducial parameters ($\xi = 100$, $T = 1.5 \times 10^5$ K) when the gas is placed at 1 pc. In Table 1 we list abundances and ionization equilibration timescales t_{ion} for commonly observed ions, calculated at ionization parameters $\xi = 30, 100, 300$, and 1000 for gas illuminated at 1 pc by a central source with an ionizing luminosity of 10^{44} erg s $^{-1}$. For these parameters, the most abundant ions have $t_{ion} \sim 10^{6 \pm 0.5}$ s. Roughly speaking, $t_{cool,ion}/t_{flow} \propto r$, so thermal and ionization equilibrium both become better approximations when the gas is clumpier and closer to the nucleus, but even at r_{max} thermal and ionization equilibrium should prevail for a substantial range of temperatures at $\Xi = \Xi_c$.

At fixed radius and pressure, both t_{cool} and t_{ion} vary along the vertical portion of the $T(\Xi)$ curve. Roughly speaking, the thermal timescale grows $\propto T^2$ at constant Ξ . At the highest temperatures, however, t_{cool} grows more rapidly as line cooling is replaced by Compton cooling. The Compton equilibration time is long enough, $\sim 10^{12} r_{pc}^2 L_{44}^{-1}$ s, that fully reaching Comptonization equilibrium is unlikely¹. Moreover, when $t_{cool} \sim t_{flow}$, adiabatic cooling can become important (as in Krolik & Begelman 1986 and Balsara & Krolik 1993). Thus, the highest temperature on the equilibrium curve reachable by gas injected cool is the temperature at which $t_{cool} \lesssim t_{flow}$, here $T_{max} \simeq 4 \times 10^6 r_{pc}^{-1/2}$ K (for distances $\gtrsim 1$ pc; at smaller distances, T_{max} approaches the Compton temperature). When the gas temperature is $\lesssim T_{max}$, it is no longer constrained to lie on the equilibrium curve; due to adiabatic cooling, it tends to move into the region of net heating.

The ionization equilibration timescale (at fixed Ξ but variable ξ or T) behaves in a somewhat more complicated fashion. It is determined by a combination of the ionizing flux and the local density. The former dominates when the ionization rate for ion j exceeds the recombination rate from j to $j - 1$, the latter when the sense of this comparison reverses. When the most abundant ion of a given element has charge $\geq j$, the former case generally applies. Because many of the species most important for soft X-ray features are H- and He-like and these elements are often mostly stripped, the former case applies more often than the latter.

Although the flux at fixed photon energy is, of course, entirely independent of T at a given radius, as the gas changes temperature, the photon energies relevant to its ionization state change. Both the photon fluxes and the cross sections can be strong functions of energy. For this reason, t_{ion} also generally rises with increasing temperature, but rather more slowly than t_{cool} —for the dominant unstripped ion of each element, t_{ion} increases by factors of $\sim 1 - 5$ from the bottom to the top of the vertical branch of the equilibrium curve.

We conclude, then, that over a wide range of possible radii, the thermal and ionization equilibration times are indeed short compared to the flow time over most of the vertical section of the thermal equilibrium curve. After a flow time, it is possible for some gas to reach high enough temperatures that it is no longer required to be in thermal balance; however, it is not necessary that all the gas reach this state. Marginal thermal stability means that the temperature of a given gas parcel can easily move either up or down on timescales $\sim t_{cool}$; all that is required is that its density change enough to compensate for the temperature change. Thus, we expect a range of temperatures to be present in this region, and also a corresponding range of densities.

2.3. Dynamics of the warm absorber

These considerations also constrain the absorber's dynamics. The absorber's equation of state is determined by how much of its material is at low enough temperature to demand thermal balance. When most of the gas is in such a state, Ξ is fixed at Ξ_c , and the pressure must vary $\propto r^{-2}$. The strength of the pressure gradient relative to gravity is then given by

$$Q = \frac{2}{\eta_{out} \Xi_c} \left(\frac{L}{L_E} \right)^{1/4} \left(\frac{\mu_e c^5}{GM \sigma_T \sigma T_c^4} \right)^{1/4} = 240 \left(\frac{L/L_E}{M_6} \right)^{1/4} \left(\frac{\Xi_c}{15} \right)^{-1} (\eta_{out} T_{c3})^{-1}. \quad (4)$$

Here η_{out} is the ratio of the mass loss rate to L/c^2 , and we suppose that r is comparable to the inner edge of the torus, where the radiation effective temperature is T_c . The fiducial parameters in Equation 4 are $10^6 M_\odot$ for the central mass M and 1000 K for T_c (the latter chosen with reference to the results of Pier & Voit 1995).

For there to be outward acceleration, $Qu > (1 - \kappa L/L_E)$, where u is the speed in free-fall units and κ is the frequency-averaged opacity in Thomson units. This condition may be regarded as an upper bound on the mass loss rate in the sense that $\eta_{out} \lesssim 240u(L/L_E)^{1/4} M_6^{-1/4}$ (assuming that radiation forces do not overcome gravity). Strikingly, this bound roughly matches the empirical estimate derived from eq. 3. In terms of the notation of that equation, $\eta_{out} = \dot{M}_{out}/(\dot{M}_{acc}\eta_{acc})$. Note, however, when making this comparison, that formally \dot{M}_{out} as estimated in equation 2 reflects only the mass loss

¹ Note that the Compton time depends on the total luminosity, not just the ionizing luminosity.

associated with matter at a single value of ξ ; if there is a distribution (as we have now argued there should be), \dot{M}_{out} is the sum of the contributions from all the components (see also §3.2).

The observed spectra suggest that the radiation pressure contribution is probably secondary. The ratio between the amount of photon momentum scattered by the wind and the total wind momentum is

$$f_{rad} = \frac{\Delta L}{L} \frac{\xi r / \Delta r}{4\pi\mu_H cv^2} = 5 \times 10^{-3} \left(\frac{\Delta L/L}{0.1} \right) \left(\frac{\xi}{100} \right) (r/\Delta r) \left(\frac{v}{500 \text{ km s}^{-1}} \right)^{-2} \left(\frac{N(\xi=100)}{N_{tot}} \right), \quad (5)$$

where the last ratio accounts for the range of ionization parameters that may be present. A scattered fraction $\Delta L/L \sim 0.1$ appears to be consistent with what is seen (Kaspi et al. 2001). Unless $\Delta r/r$ is quite small, f_{rad} is likely to be well less than unity.

The pressure in the wind is $\propto \langle T \rangle \dot{M} (u/r^{1/2})^{-1} r^{-2}$, where $\langle T \rangle$ is the mean temperature. Fixed Ξ then requires $\langle T \rangle \dot{M} (u/r^{1/2})^{-1}$ to be constant. If \dot{M} were constant (which is not strictly required due to possible continuing evaporation or condensation), the velocity (and $\langle T \rangle$) would increase only logarithmically with r . However, because the gas dynamics depend on its pressure, not its temperature, there is no requirement for the temperature to rise smoothly and homo-

TABLE 1
EQUILIBRATION TIMES FOR SELECTED IONS

Ion	$\xi = 30$		$\xi = 100$		$\xi = 300$		$\xi = 1000$	
	A	τ_{eq} (s)	A	τ_{eq} (s)	A	τ_{eq} (s)	A	τ_{eq} (s)
H I	1.03×10^{-7}	2.79×10^1	1.10×10^{-8}	2.72×10^1	1.26×10^{-9}	2.75×10^1	1.86×10^{-10}	2.83×10^1
He II	2.42×10^{-7}	2.75×10^3	2.68×10^{-8}	2.72×10^3	3.17×10^{-9}	2.53×10^3	5.14×10^{-10}	2.62×10^3
C III	5.34×10^{-9}	1.46×10^3	2.54×10^{-12}	1.43×10^3	4.20×10^{-16}	1.32×10^3
C IV	2.37×10^{-7}	6.70×10^3	5.80×10^{-10}	6.66×10^3	1.43×10^{-12}	6.07×10^3	1.40×10^{-14}	6.24×10^3
C V	2.49×10^{-5}	6.92×10^4	5.62×10^{-7}	6.93×10^4	1.31×10^{-8}	6.96×10^4	5.02×10^{-10}	7.04×10^4
C VI	4.10×10^{-5}	2.44×10^5	9.57×10^{-6}	2.45×10^5	1.38×10^{-6}	2.46×10^5	2.49×10^{-7}	2.49×10^5
N V	9.76×10^{-7}	1.75×10^4	4.94×10^{-9}	1.75×10^4	1.22×10^{-11}	1.66×10^4	8.58×10^{-14}	1.65×10^4
N VI	2.20×10^{-5}	1.30×10^5	9.63×10^{-7}	1.30×10^5	2.29×10^{-8}	1.30×10^5	9.14×10^{-10}	1.32×10^5
N VII	3.86×10^{-4}	4.21×10^5	1.65×10^{-4}	4.21×10^5	2.69×10^{-5}	4.23×10^5	4.98×10^{-6}	4.28×10^5
O VI	3.87×10^{-5}	3.03×10^4	5.38×10^{-7}	3.04×10^4	1.62×10^{-9}	2.98×10^4	1.13×10^{-11}	2.94×10^4
O VII	3.31×10^{-4}	2.24×10^5	3.81×10^{-5}	2.24×10^5	1.06×10^{-6}	2.25×10^5	4.25×10^{-8}	2.28×10^5
O VIII	4.87×10^{-5}	3.24×10^6	4.46×10^{-5}	6.78×10^5	9.18×10^{-6}	6.80×10^5	1.77×10^{-6}	6.89×10^5
Ne VIII	3.17×10^{-5}	7.88×10^4	2.10×10^{-6}	7.89×10^4	1.37×10^{-8}	7.91×10^4	1.18×10^{-10}	7.91×10^4
Ne IX	5.74×10^{-5}	5.27×10^5	3.47×10^{-5}	5.28×10^5	1.83×10^{-6}	5.30×10^5	8.18×10^{-8}	5.37×10^5
Ne X	3.46×10^{-6}	1.49×10^6	1.86×10^{-5}	1.49×10^6	8.81×10^{-6}	1.50×10^6	2.01×10^{-6}	1.52×10^6
Mg XI	6.33×10^{-6}	1.08×10^6	1.90×10^{-5}	1.08×10^6	3.43×10^{-6}	1.08×10^6	2.21×10^{-7}	1.10×10^6
Mg XII	3.40×10^{-7}	2.84×10^6	8.61×10^{-6}	2.85×10^6	1.51×10^{-5}	2.86×10^6	4.91×10^{-6}	2.89×10^6
Si XIII	9.34×10^{-7}	1.98×10^6	1.01×10^{-5}	1.99×10^6	9.50×10^{-6}	1.99×10^6	1.09×10^{-6}	2.02×10^6
Si XIV	1.27×10^{-8}	4.91×10^6	1.03×10^{-6}	4.90×10^6	1.04×10^{-5}	4.92×10^6	5.89×10^{-6}	4.99×10^6
S XV	4.75×10^{-8}	3.29×10^6	1.72×10^{-6}	3.29×10^6	9.44×10^{-6}	3.31×10^6	2.22×10^{-6}	3.35×10^6
S XVI	6.38×10^{-11}	2.97×10^{12}	1.82×10^{-8}	7.89×10^6	1.17×10^{-6}	7.92×10^6	1.36×10^{-6}	8.03×10^6
Ar XVII	3.32×10^{-10}	5.03×10^6	8.07×10^{-8}	5.04×10^6	1.51×10^{-6}	5.05×10^6	7.71×10^{-7}	5.12×10^6
Ar XVIII	9.05×10^{-13}	1.05×10^6	1.85×10^{-9}	1.20×10^7	4.32×10^{-7}	1.20×10^7	1.08×10^{-6}	1.22×10^7
Ca XIX	2.79×10^{-12}	7.58×10^6	3.85×10^{-9}	7.58×10^6	4.06×10^{-7}	7.61×10^6	9.02×10^{-7}	7.71×10^6
Ca XX	8.36×10^{-14}	2.32×10^3	9.17×10^{-10}	1.89×10^7	1.19×10^{-6}	1.75×10^7	1.29×10^{-5}	1.77×10^7
Fe XVI	6.35×10^{-6}	1.25×10^5	1.43×10^{-6}	1.25×10^5	1.45×10^{-8}	1.26×10^5	4.06×10^{-13}	1.27×10^5
Fe XVII	4.35×10^{-6}	1.78×10^5	9.40×10^{-6}	1.78×10^5	6.48×10^{-7}	1.79×10^5	7.61×10^{-11}	1.81×10^5
Fe XVIII	6.71×10^{-7}	2.57×10^5	9.24×10^{-6}	2.58×10^5	4.33×10^{-6}	2.59×10^5	3.73×10^{-9}	2.62×10^5
Fe XIX	5.66×10^{-8}	2.72×10^5	3.81×10^{-6}	2.72×10^5	8.05×10^{-6}	2.73×10^5	4.84×10^{-8}	2.76×10^5
Fe XX	5.27×10^{-9}	4.92×10^5	1.32×10^{-6}	4.93×10^5	1.08×10^{-5}	4.95×10^5	5.50×10^{-7}	5.01×10^5
Fe XXI	1.26×10^{-10}	3.86×10^5	1.06×10^{-7}	3.86×10^5	3.66×10^{-6}	3.88×10^5	1.13×10^{-6}	3.92×10^5
Fe XXII	4.05×10^{-8}	9.96×10^5	3.04×10^{-6}	1.00×10^6	4.83×10^{-6}	1.01×10^6
Fe XXIII	4.62×10^{-9}	2.15×10^6	8.39×10^{-7}	2.16×10^6	6.88×10^{-6}	2.18×10^6
Fe XXIV	1.08×10^{-10}	3.50×10^6	1.00×10^{-7}	3.51×10^6	5.09×10^{-6}	3.55×10^6
Fe XXV	6.15×10^{-8}	2.08×10^7	1.07×10^{-5}	2.11×10^7
Fe XXVI	2.50×10^{-9}	4.68×10^7	2.20×10^{-6}	4.64×10^7

Note. — Abundances relative to hydrogen (A) and equilibration timescales (τ_{eq}) for selected ions of the most astrophysically-abundant elements in thermal balance at photoionization parameters of $\xi = 30, 100, 300, 1000$ assuming a distance of $r = 1$ pc from a source of luminosity 10^{44} erg s $^{-1}$. The computations were done using XSTAR Version 2.1.

generously so long as $\Xi = \Xi_c$. Temperature fluctuations with wavelengths shorter than r and long enough that thermal conduction does not damp them can be easily created. We would expect, therefore, that, although there may be an overall sense of temperature evolution, there can be substantial local inhomogeneity. Eventually, the approximation made at the beginning that $\Xi = \Xi_c$ must break down. As Compton equilibrium is neared, the equilibrium Ξ begins to increase and the requirement of tracking the equilibrium curve is weakened as t_{cool} approaches and then exceeds t_{flow} .

3. COMPARISON WITH OBSERVATIONS

3.1. Inferred ionization parameters and temperatures

As we have just seen, this model predicts that the distribution of Ξ in this gas should be very narrow, but the temperature distribution is likely to be much wider. In a fashion strikingly consistent with these predictions, Kaspi et al. (2001) found it impossible to adequately fit their data with only a single component. Moreover, their two inferred components lie squarely on the vertical section of the equilibrium curve, one near 8×10^4 K, the other at $\simeq 6 \times 10^5$ K. The similarity of all the line profiles suggests that these two components are subject to more or less the same forces, and are therefore not very distant from each other. Because they have the same value of Ξ , if they lie at similar distances from the central source, their pressures must also be the same. Only if there is global pressure-confinement (i.e., a volume-filling background medium) would one expect these pressures to match.

Our model predicts temperatures across a somewhat wider range, from $\simeq 3 \times 10^4$ K up to $\sim 10^6$ K. It may be difficult to detect the hottest gas, however. As one can see in Table 1, only for elements with atomic number ≥ 12 (Mg and above) do more than 10% of the atoms retain at least one electron when $\xi = 1000$ ($T \simeq 9 \times 10^5$ K); only a small increase in temperature beyond that point suffices to eliminate almost all the unstripped ions except Fe. In the band covered by the Chandra gratings, only two lines in gas with $\xi \simeq 1000$ (Fe XXII 10.98,11.77) can be expected to have line-center optical depths greater than unity when the velocity span is 500 km s^{-1} and the column density is 10^{22} cm^{-2} (although another half dozen lines have opacities a factor of two smaller). Moreover, because the H-like stages of Mg, Si, S, Ar begin to be abundant when $T > 5 \times 10^5$ K, it can be hard to distinguish 10^6 K gas from gas at half that temperature.

UV features, on the other hand, grow in opacity at the lowest temperatures. For example, Table 1 shows that the fractional abundances² of C IV and O VI relative to H rise from 5.8×10^{-10} and 5.4×10^{-7} , respectively, at $\xi = 100$ (1.5×10^5 K) to 2.4×10^{-7} and 3.9×10^{-5} at $\xi = 30$ (4.7×10^4 K). Any significant amount of gas at the low end of the temperature range is then likely to generate UV absorption features. These are, in fact, often observed. In order to produce the line strengths seen, not much is required: for typical cases (Crenshaw et al. 1999; Kriss et al. 2000; Kaiser et al. 2001), $\lesssim 10^{19} \text{ H cm}^{-2}$ suffices if the gas temperature is 5×10^4 K.

3.2. Clumping

If there is nothing to restrain it, there is no reason why this gas should not expand to fill the volume available to it. In fact, if the absorber gas were not volume-filling, one would have to ask what gas occupied the remainder of the region, and that gas would be subject to the same thermodynamic constraints as the gas under consideration. Within this volume, however, there are no obvious constraints favoring any particular temperature from $\simeq 3 \times 10^4$ K up to the maximum temperature achievable within a flow time, a few $\times 10^6$ K.

We do not know how to predict the distribution of column density with temperature dN/dT . Once it is given, though, we can find the distribution of volume with temperature: A differential column density dN having volume density n occupies a radial shell with thickness $d\Delta r = dN/n$. In terms of the pressure p , $d\Delta r = (kT/p)dN$, so that the distribution of fractional volume with temperature $d(\Delta r/r)/dT \propto TdN/dT$. The normalization of this relation is fixed by the constraint $\int dT d(\Delta r/r)/dT = 1$. That is, for equal column density and fixed pressure, higher temperature regions occupy larger volumes.

Given a particular distribution dN/dT , it is possible to predict the distance of the entire system from the central continuum source. Suppose, for example, that $dN/d\log T$ is constant from $T_{min} = 3 \times 10^4$ K up to $T_{max} = 10^6$ K. Because $\xi \propto \Xi/T$, from Equation 1 it then follows that the distance at which this material exists is

$$r_{pred} \simeq \frac{L_{ion} \log(T_{max}/T_{min})}{4\pi c \Xi_c k T_{max} N_{tot}} \simeq 4L_{ion,44} \left(\frac{N_{tot}}{3.5 \times 10^{22} \text{ cm}^{-2}} \right)^{-1} \left(\frac{\Xi_c}{15} \right)^{-1} \left(\frac{T_{max}}{1 \times 10^6 \text{ K}} \right)^{-1} \text{ pc}, \quad (6)$$

where N_{tot} is the total column density, approximately a factor of 3.5 greater than the column density per $\log T$. Unfortunately, this estimate is rather model-dependent because we have no way of determining the true dN/dT . In particular, to the degree that the higher temperatures have larger column densities, r_{pred} would decrease. However, this example does emphasize the likelihood that gas at intermediate T occupies only a fraction of the volume.

3.3. Variability

For considerations of bulk dynamics, ionization balance is a good approximation when $t_{ion} < t_{flow}$. However, because we can observe changes on timescales much shorter than t_{flow} , it is possible for us to see continuum fluctuations driving short-lived changes in the ionization balance. In fact, because the observed continuum flux and the absorption features “ride the light-cone” together, we can even follow fluctuations on timescales much shorter than the light-crossing time.

² XSTAR uses the elemental abundances of Grevesse et al. 1996.

The column densities we measure reflect the history of the continuum flux over the past t_{ion} ; the temperature inferred from column densities is the product of heating and cooling over the past t_{cool} .

The relation between observed absorption column densities and the continuum provides an excellent diagnostic of the actual distance between the continuum source and the gas. At a distance of 1 pc, Table 1 shows $t_{ion} \sim 10^{6\pm 0.5}$ s for those species most visible in the soft X-ray band. However, since $t_{ion} \propto r^2$, the magnitude of t_{ion} depends sensitively on the column density in the hottest (and nearly transparent) component. For example, if the guess illustrated in equation 6 is correct, the true distance would be $\simeq 4$ times larger, making the ionization timescales $\simeq 16$ times longer, or $10^{7.2\pm 0.5}$ s for the species creating soft X-ray features. UV features should respond somewhat more quickly. Although it may be very difficult to monitor AGN X-ray lightcurves with sampling density sufficient to quantitatively match continuum fluctuations with ionization fluctuations, it should at least be possible to estimate upper bounds on ionization response times. These bounds can then provide constraints on the distance to this material, and, in this model, dN/dT .

As of now, there has been little in the way of systematic monitoring of warm absorbers. The clearest report in the literature of very rapid changes in an absorbing column is an apparent sharp increase in the O VIII K-edge optical depth in MCG-6-30-15 that occurred in a span of $\sim 10^4$ s during an ASCA observation (Reynolds et al. 1995; Otani et al. 1996). Within the context of our model, this time could be brought into agreement with the observed time if there were a column density $\simeq 2 \times 10^{23}$ H cm $^{-2}$ in gas at $T \gtrsim 10^6$ K. However, it is also possible that this feature may have been confused with O VIII K α emission broadened by relativistic motions in the accretion disk (Branduardi-Raymont et al. 2001). The fact that when the O VIII column density in MCG-6-30-15 increased, the measured O VII column density was constant may support this alternate interpretation. A somewhat similar event occurred in NGC 4051, but with the roles of O VII and O VIII reversed—the O VII column density changed while the O VIII column density was constant (Guainazzi et al. 1996). In this case, because the luminosity of the nucleus is so small ($\sim 10^{42}$ erg s $^{-1}$), the timescale— $\sim 10^4$ s—places only a weak upper bound on the distance, $r \lesssim 0.2$ pc. This is, of course, easily consistent with estimates like equation 6.

Evidence in the UV to date is similarly fragmentary. Kriss et al. (1997) reported Lyman edge optical depth changes in NGC 4151, and Espey et al. (1998) saw C III column density changes in the same object that anti-correlated with the continuum flux on timescales of days. Unfortunately, the X-ray absorption in NGC 4151 is so complex that the warm absorber column density cannot be estimated well enough for us to predict the ionization timescale.

3.4. Emission lines and the covering factor

The peculiar geometry of flow through the opening in toroidal obscuration means that we cannot see the entire emission portion of P Cygni profiles created by absorption lines. In part this is because at many radii the warm ionized gas simply does not fill all solid angle (most of it is occupied by the dusty, molecular obscuring gas); in part this is because the obscuring matter partially blocks our view of the far side of the flow. In line with this prediction, Kaspi et al. (2001) use the P Cygni features they discovered in the spectrum of NGC 3783 to estimate covering fractions of $\simeq 0.3$ and $\simeq 0.5$ for their high- and low-ionization components, respectively.

Unless $r \ll r_{max}$, variations in the column densities of the emission components on the timescale of continuum fluctuations (days to weeks) should be averaged out because the light-crossing time is much longer (several years). Consequently, the covering fraction inferred on the basis of a single “snap-shot” may not be a fair measure of the true covering fraction.

4. SUMMARY

A wide variety of evidence now points toward locating the gas that produces ionized absorption features in the soft X-ray spectra of AGN in a warm wind that lies a few parsecs from the nucleus in Seyfert galaxies. Both absorption and emission lines are seen with widths of ~ 500 km s $^{-1}$, in many cases with the telltale “P Cygni” velocity shifts. The inferred ionization parameters and column densities indicate maximum distances ~ 30 pc.

The specific ionization states indicated by the observed lines suggest that there are a number of components with different values of ξ , the density form of the ionization parameter. However, these all have the same value ($\Xi = \Xi_c$) of the pressure form of the ionization parameter. Above Ξ_c , low-temperature equilibria do not exist, and the temperature rises from $\simeq 3 \times 10^4$ K to $\simeq 10^6$ K with Ξ very nearly constant at Ξ_c . If these components coexist at the same distance from the central source, they share the same pressure, suggesting a volume-filling configuration by which the pressure is regulated. If the volume-filling phase is the highest attainable temperature on the marginally stable branch of the thermal equilibrium curve, the actual distance could be substantially smaller than the maximum; a factor of ten smaller would not be surprising.

Because the thermal equilibria at $\Xi = \Xi_c$ are marginally stable to fixed-pressure thermal perturbations, material can move easily from one temperature to another. The only constraint is that accessible temperatures must have thermal equilibration times short compared to the flow time. Consequently, we expect that multi-temperature models will in general be required in order to explain all the observed features.

Given that a very similar wind in a very similar location has been previously inferred from the scattering of nuclear light in obscured Seyfert galaxies, it makes sense to suppose that the two are essentially the same structure. However, absorption features in type 1 Seyfert galaxy X-ray spectra provide much more sensitive diagnostics of its state than does the polarized reflection of the continuum that can be observed in type 2 Seyfert galaxies. In particular, the time-dependent response of the absorbing column densities as the X-ray continuum level changes should provide a very sensitive test of these ideas.

We would like to thank Mike Crenshaw for organizing the workshop “Mass Outflow in Active Galaxies: New Perspectives”, whose discussions provoked some of these thoughts. We are also indebted to Tim Kallman for creating and maintaining the new version of XSTAR. This work was partially supported by NASA Grant NAG5-9187 to JHK.

REFERENCES

- Antonucci, R.R.J. 1993, *ARA&A*, 31, 473
 Balsara, D.S. & Krolik, J.H. 1993, *ApJ* 402, 109
 Bottorff, M., Korista, K. & Shlosman, I. 2000, *ApJ* 537, 134
 Brandt, W.N., Mathur, S., Reynolds, C.S. & Elvis, M. 1997, *MNRAS* 292, 407
 Branduardi-Raymont, G., Sako, M., Kahn, S. M., Brinkman, A.C., Kaastra, J.S., & Page, M. J. 2001, *in press* (astro-ph/0011167)
 Collinge, M. et al. 2001, astro-ph/0104125
 Crenshaw, D. M., Kraemer, S. B., Boggess, A., Maran, S. P., Mushotzky, R. F., Wu, C.-C. 1999, *ApJ*, 516, 750
 Elvis M., *ApJ*, 545, 63
 Espey, B.R., Kriss, G.A., Krolik, J. H., Zheng, W., Tsvetanov, Z., & Davidsen, A.F. 1998, *ApJ*, 500, L13
 George, I. M., Turner, T. J., Netzer, H., Nandra, K., Mushotzky, R. F., & Yaqoob, T. 1998, *ApJS*, 114, 73
 George, I.M., Turner, T.J., Yaqoob, T., Netzer, H., Laor, A., Mushotzky, R.F., Nandra, K., & Takahashi, T. 2000, *ApJ* 531, 52
 Greenhill, L.J., Gwinn, C.R., Antonucci, R.R.J. & Barvainis, R. 1996, *ApJ* 472, L21
 Grevesse, Noels & Sauval 1996, in *Cosmic Abundances*, ASP Conf. 99, eds. S. Holt & G. Sonneborn (San Francisco:ASP)
 Guainazzi, M., Mihara, T., Otani, C. & Matsuoka, M. 1996, *P.A.S.J.* 48, 781
 Kaastra, J. S., Mewe, R., Liedahl, D. A., Komossa, S., Brinkmann, A. C. 2000, *A&A*, 354, L83
 Kaiser, M.E. et al. 2001, *ApJ* in preparation
 Kallman, T.R. 2000, heasarc.gsfc.nasa.gov/docs/software/xstar/docs/html/xstarmanual.html
 Kaspi, S., Brandt, W. N., Netzer, H., Sambruna, R., Chartas, G., Garmire, G. P. & Nousek, J. A. 2000, *ApJ*, 535, L17
 Kaspi, S., Brandt, W. N., Netzer, H., George, I., Chartas, G., Behar, E., Sambruna, R., Garmire, G. P. & Nousek, J. A. 2001, *ApJ* 554, 216
 Kriss, G., Krolik, J., Grimes, J., Tsvetanov, Z., Zheng, W., & Davidsen, A. 1997, in *proc. IAU Colloquium 159*, A.S.P. Conf. Series, V. 113, ed. B.M. Peterson, F.-Z. Cheng, & A.S. Wilson (San Francisco: ASP), 453
 Kriss, G. A., et al. 2000, *ApJ*, 538, L17
 Krolik, J.H., & Begelman, M.C. 1986, *ApJ*, 308, L55
 Krolik, J. H., & Kriss, G. A. 1995, *ApJ*, 447, 512
 Krolik, J.H. & Lepp, S. 1989, *ApJ* 347, 179
 Krolik, J.H. & London, R.A. 1983, *ApJ* 267, 18
 Krolik, J.H., McKee, C.F., & Tarter, C.B. 1981, *ApJ*, 249, 422
 Lee, J. L., Ogle, P. M., Canizares, C. R., Marshall, H. L., Schulz, N. S., Morales, R., Fabian, A. C., & Iwasawa, K. 2001, (astro-ph/0101065)
 Mathur, S., Wilkes, B., & Elvis, M. 1995, *ApJ*, 452, 230
 Mathur, S., Wilkes, B., Elvis, M., & Fiore, F. 1994, *ApJ*, 434, 493
 Mathur, S., Wilkes, B.J. & Aldcroft, T. 1997, *ApJ* 478, 182
 McHardy, I., Green, A.R., Done, C., Puchnarewicz, E.M., Mason, K.O., Branduardi-Raymont, G. & Jones, M.H. 1995, *MNRAS* 273, 549
 Morales, R.F., Fabian, A.C., & Reynolds, C.S. 2000, *MNRAS* 315, 149
 Netzer, H. 1993, *ApJ*, 411, 594
 Netzer, H. 1996, *ApJ*, 473, 781
 Netzer, H. 1997, in *IAU Coll. 159: Emission Lines in Active Galaxies: New Methods and Techniques*, B.M. Peterson, F.-Z. Cheng & A.S. Wilson, eds. (San Francisco, ASP), p. 20
 Neufeld, D.A., Maloney, P.R. & Conger, S. 1994, *ApJ* 436, L127
 Otani, C., et al. 1996, *PASJ*, 48, 211
 Pier, E.A., Antonucci, R., Hurt, T., Kriss, G. & Krolik, J. 1994, *ApJ* 428, 124
 Pier, E.A. & Voit, G.M. 1995, *ApJ* 450, 628
 Proga, D., Stone, J.M. & Kallman, T.R. 2000, *ApJ* 543, 686
 Reichert, G.A. et al. 1994, *ApJ* 425, 582
 Reynolds, C. S. 1997, *MNRAS*, 286, 513
 Reynolds, C.S., Fabian, A.C., Nandra, K., Inoue, H., Kunieda, H., Iwasawa, K. 1995, *MNRAS* 277, 901
 Turner, T.J., Nandra, K., George, I.M., Fabian, A.C. & Pounds, K. 1993, *ApJ* 419, 127